Digital Mammography: From Physical Performance Evaluation To Image Quality Analysis

Anastasios C. Konstantinidis

Department of Medical Physics and Bioengineering, University College London, UK.

taskon25@yahoo.gr

Abstract

Since the early 1990s digital X-ray detectors have been used extensively for medical imaging applications, such as Mammography, General Radiography, Computed Tomography, Tomosynthesis, Fluoroscopy, etc. The quality of a radiograph needs to be adequate to provide the required information for a given task. The primary physical parameters that affect image quality are spatial resolution, noise, and contrast. The Modulation Transfer Function (MTF) is the combination of contrast and resolution, the Noise Power Spectrum (NPS) combines the noise and resolution, and the Signal-to-Noise Ratio (SNR) expresses the ratio between signal and noise in large scale objects (i.e. at zero spatial frequency). The combination of SNR, MTF and NPS determines the Detective Quantum Efficiency (DQE) which represents the ability to visualize object details of a certain size and contrast. This study is using image simulation to estimate how the experimentally measured SNR, MTF and NPS of several digital X-ray detectors affect the mammographic image quality. The latter is measured in terms of Contrast-to-Noise Ratio (CNR) and Contrast-Detail (CD) analysis, using synthetic breast and CDMAM phantoms, respectively.

Key words: Digital X-ray detectors, Physical Performance, Modulation Transfer Function, Noise Power Spectrum, Mammography, Image Quality

Introduction

Medical X-ray imaging is used to provide useful information about specific aspects of human body structure or function. The quality of a radiograph needs to be sufficient to provide the required information for a given imaging task. Image quality is mainly affected by a) spatial resolution, b) noise, and c) contrast. All three parameters need to reach sufficient levels to get meaningful images for a given task. The spatial resolution expresses the ability of a detector to represent distinct anatomic features within the object being imaged. The noise describes systematic and random variations superimposed on the actual measured signal, arising from the X-ray photons and the detector itself. The contrast is the magnitude of the relative signal difference between the object of interest and the surrounding background[1,2]. The Modulation Transfer Function (MTF) is the combination of contrast and resolution, the Noise Power Spectrum (NPS) combines the noise and resolution, and the Contrast-to-Noise Ratio (CNR) is the ratio between contrast and noise. The Signal-to-Noise Ratio (SNR) is another useful parameter and expresses the ratio between signal and noise in large scale objects (i.e. at zero spatial frequency). The combination of SNR, MTF and NPS determines the Detective Quantum Efficiency (DQE) which represents the ability of an X-ray detector to represent object details of a certain size and contrast[3].

The objective X-ray performance evaluation parameters (i.e. MTF, NPS and

DQE) can be used to compare the performance of different X-ray detectors. However, these parameters can not be directly used to predict image quality because they do not involve the radiologists, radiographers or patients (i.e. subjective evaluation). Since image quality is task dependent we can not easily predict whether it is more strongly affected by spatial resolution (MTF) or noise (NPS)[4]. To overcome this limitation, the experimentally measured X-ray performance parameters (i.e. MTF, NPS and SNR) of six digital mammographic X-ray detectors[5,6] were combined with ideal software phantoms to get simulated mammograms. In particular, a modified version of Saunders and Samei[4] algorithm was used [5,7] to predict and compare the mammographic image quality of the investigated X-ray detectors using ideal software phantoms of two categories: a) two three dimensional (3-D) breasts [8,9] of different thickness (6 and 5 cm) and glandularity (45 and 73 %) to estimate the CNR between simulated microcalcifications (μCas) and the adjacent background, and b) the Artinis CDMAM 3.4 test tool[10] for a contrast-detail analysis of small thickness and low contrast objects[11].

Materials and Methods

Mammographic detectors are either analog (screen-film (SF)) or digital (Digital Radiography (DR) or Computed Radiography (CR)). DR detectors have better performance than CR ones[12] and are mainly based on Thin Film Transistor (TFT), Charge-Couple Device (CCD), and Complementary Metal Oxide Semiconductor (CMOS) technologies[13, 14]. TFT-based detectors are direct (Amorphous Selenium (a-Se)) or indirect (Amorphous Silicon (a-Si:H)) conversion detectors. On the other hand, CMOS detectors are indirect conversion detectors, based on either Active Pixel Sensor (APS) or Passive Pixel Sensor (PPS) technology. Figure 1 shows the main categories of mammographic detectors.
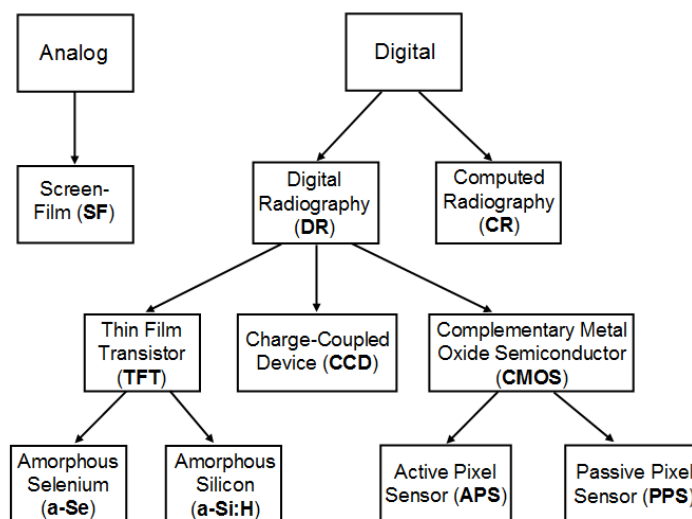

Figure 1. X-ray detectors used in Mammography

The investigated mammographic detectors were a) LAS (Large Area Sensor, CMOS APS, 40 μm pixel pitch, coupled to 150 μm Cesium Iodide (CsI:Tl) scintillator), b) Hamamatsu C9732DK (CMOS PPS, 50 μm pixel pitch, coupled to 150 μm CsI), c) Anrad SMAM (a-Se TFT, 85 μm pixel pitch), d) Dexela 2923 MAM (operated in High Full Well (HFW) mode, CMOS APS, 74.8 μm pixel pitch, coupled to 150 μm CsI), e) Remote RadEye HR (CMOS APS, 22.5 μm pixel pitch, coupled to 85 μm Gadolinium Oxysulfide (Gd2O2S:Tb) scintillator), and f) DynAMITe

(Dynamic range Adjustable for Medical Imaging Technology, CMOS APS, operated in Sub-Pixel (SP) camera mode (50 μm pixel pitch), coupled to 150 μm CsI). Further details about the investigated detectors can be found elsewhere[5,6,15,16]. Figure 2 shows photographs of the investigated detectors.

The DQE expresses the ability of an X-ray detector to transfer the Signal-to-Noise Ratio (SNR) from its input to output. It expresses the fraction of input X-ray photons used to create an image at each spatial frequency and describes the ability of a particular system to effectively use the available input quanta:

$$DQE(\,f\,) = \frac{SNR_{out}^2}{SNR_{in}^2} = \frac{pMTF^2(\,f\,)}{\Phi \cdot NNPS(\,f\,)} \tag{1}$$

where Φ is the photon fluence (expressing the SNR2 input in X-rays/mm2), pMTF is the presampling Modulation Transfer Function, and NNPS is the Normalized Noise Power Spectrum. The measurements and calculations of pMTF, NNPS and DQE were made at 28 kV using Tungsten/Aluminum (W/Al) anode/filtration combination according to the mammographic IEC standard[17].
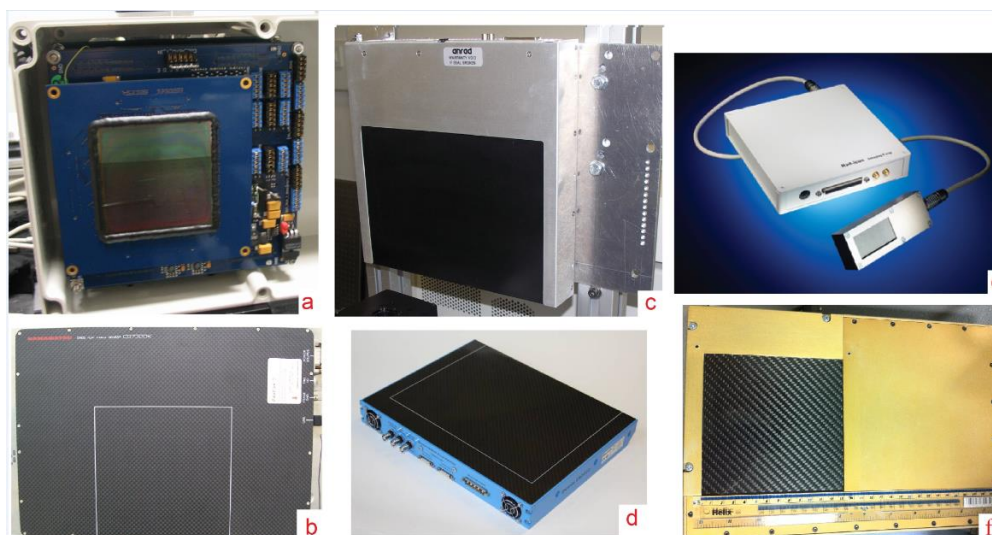
Figure 2. Photographs of a) LAS, b) Hamamatsu C9732DK, c) Anrad SMAM, d) Dexela 2923MAM, e) Remote RadEye HR, and f) DynAMITe

In order to simulate the mammographic image quality, a modified algorithm of Saunders and Samei method[4] was used[5,7]. Briefly, the two dimensional (2-D) pMTF matrix of a digital X-ray detector was multiplied with an ideal input image in the frequency domain to insert blurring. Then an inverse Fourier transform was applied to the product and the blurred image was sampled to form the pixels of the digital image. The measured NNPS distribution was used to create a flat image with noise. This noise image was rescaled at specific Air Kerma at Detector surface (DAK) level and added to the blurred and sampled object image to form the final simulated image.

In order to calculate the CNR, two breast software phantoms (based on [8,9]) of different composition (45 and 73 % glandularity) and thickness (6 and 5 cm, respectively) were used as ideal input images. In a few words, the ideal software phantoms are 2-D X-ray projection images (at craniocaudal (CC) orientation) of compressed 3-D software breasts containing the breast external shape, skin, mammary duct system, breast abnormalities, mammographic texture, Cooper's ligaments,

pectoralis muscle, lymphs, and blood vessels. Both breast phantoms contained CaCO3 spheres with 0.6 mm diameter to simulate μCas. The 3-D breast models were reconstructed as 2-D projection images at 90 degrees angle to generate a set of line integrals with 10 μm "analog" pitch[5]. Table I shows the main parameters related to the ideal software breast phantoms. It should be noted that the synthetic mammograms correspond to two distinct Entrance Surface Air Kerma (ESAK) levels: 2 and 5.5 mGy. However, the different composition and thickness of each breast results in four different DAK levels: 46.7 and 128.5 μGy for Breast 1, and 32.5 and 89.3 μGy for Breast 2. It should be noted that the average DAK level in Mammography is in the range 100-120 μGy[5]. However, LAS saturates at around 60 μGy (due to high sensitivity). Hence, we decided to measure the mammographic image quality at low and high DAK levels.

Table 1. Parameters related to the synthetic breast phantoms

Parameter	Breast 1	Breast 2	Unit
Thickness	5	6	cm
Granularity	73	45	%
μCa diameter	0.6	0.6	mm
Low DAK	46.7	32.5	μGy
High DAK	128.5	89.3	μGy

Figure 3 shows a synthetic mammogram with six μCa discs. To implement the CNR analysis, circular regions of interest (ROIs) were extracted from the center of each disc. The size of the ROI was selected in order to be in the central area of the disc and four circular ROIs were selected from adjacent background areas with diameter three times larger than that of the disc ROI. This happens to take into account the variations of the background. The CNR was calculated as follows:

$$CNR = \frac{m_o - m_b}{\sqrt{\dfrac{\sigma_o^2 + \sigma_b^2}{2}}} \qquad (2)$$

where m_o and m_b are the average digital numbers (DN) of the object of interest and the surrounding background, and σ_o and σ_b are the respective average standard deviations (in DN).
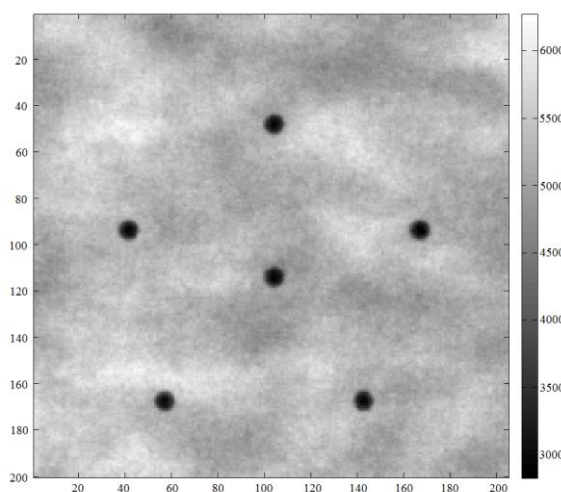
Figure 3. Region of synthetic mammogram

In order to apply contrast-detail (CD) analysis, a software Artinis CDMAM 3.4 test tool[10,18] was used. It should be noted that contrast-detail analysis is used to measure the ability of an X-ray system to detect low contrast and small details. In other words, it takes into account the combination of resolution, contrast and noise. The CDMAM 3.4 phantom consists of a 16 cm x 24 cm x 0.3 mm Al plate with 205 square cells (arranged in 16 rows x 16 columns). Each cell contains two identical gold discs (one at the center and one in a randomly chosen corner - eccentric disc) of given thickness and diameter that decrease logarithmically to cover a range of object diameters from 2.00 to 0.06 mm in each column and thicknesses between 2.00 and 0.03 mm in each row[18]. The CDMAM 3.4 test tool (Figure 4) is used to determine the contrast limit (threshold contrast) or threshold thickness for a given disc diameter that corresponds to successful observation of the eccentric disc location.
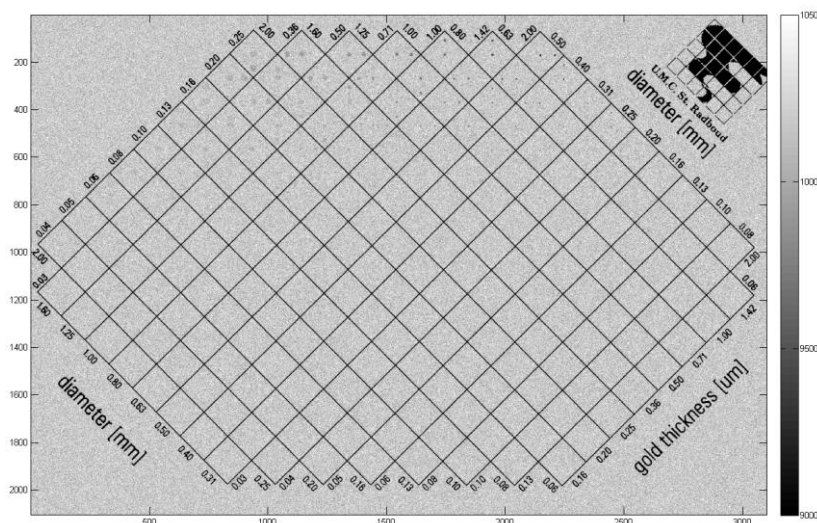

Figure 4. Simulated radiograph of the CDMAM 3.4 test tool

The evaluation of the CDMAM 3.4 test tool radiographs was made using the freeware CDCOM 1.5.2 software tool[19]. Further analysis, based on the psychometric curve fit[20], was made to calculate the threshold thickness for a given diameter. A MATLAB-based Graphical User Interface (GUI) software (namely CDMAM_fit_3[21]) was used to apply psychometric curve fit[11].

Results and Discussion

Figure 5a shows the Signal Transfer Property (STP) curves (i.e. the output average signal (in DN) as a function of the input DAK (in µGy)) of the investigated X-ray detectors. It should be noticed that LAS has the highest sensitivity (i.e. it saturates at low DAK levels), while the Remote RadEye HR detector has the lowest one. Figure 5b demonstrates the average pMTF values of the detectors. Anrad SMAM detector has the highest pMTF values (because it is a direct conversion detector) while LAS has the lowest ones (due to unoptimised scintillator coupling). It should be noted that Hamamatsu, Dexela and DynAMITe SP detectors have similar pMTF values (mainly in the frequency range 2.5-6 line pairs per millimeter (lp/mm)).
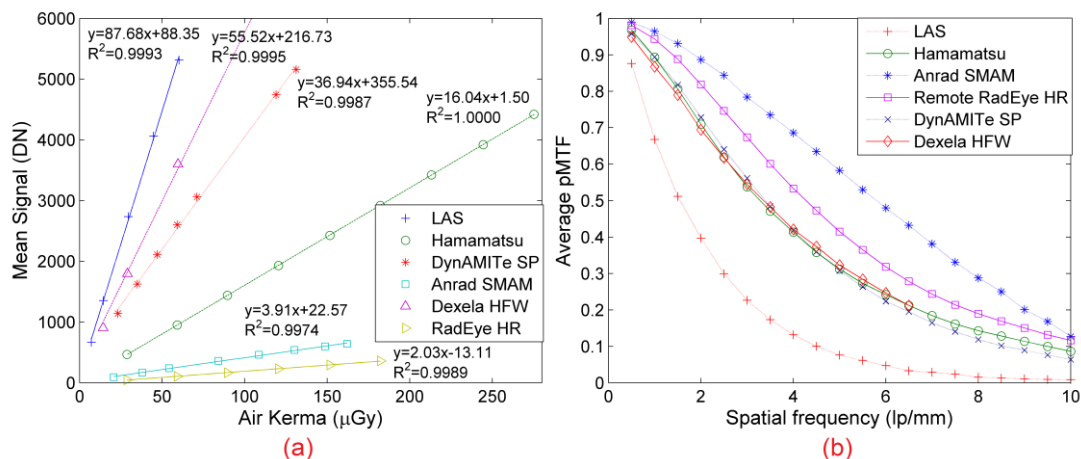
**Figure 5.** a) STP curves and b) average pMTF curves of the investigated X-ray detectors at 28 kV (W/Al)

Figure 6 shows the average DQE values of the X-ray detectors. It can be observed that LAS has high DQE values (around 0.7) at 0.5 lp/mm (DQE(0.5) and low DQE values at higher ones (due to low pMTF values). Hamamatsu has medium DQE values at low spatial frequencies (around 0.45 at 0.5 lp/mm). Anrad SMAM has high DQE(0.5) values but the DQE drops at high spatial frequencies due to aliasing (which is common within direct conversion detectors). The Dexela detector has relatively high DQE values in almost the whole frequency range. This happens due to the relationship between signal and noise, i.e. the ratio between pMTF and NNPS. DynAMITe SP has relatively high DQE(0.5) values (around 0.65) and lower ones at higher spatial frequencies. Finally, Remote RadEye HR has the worst DQE values (less than 0.4), so it was decided to exclude this detector from the image simulation.
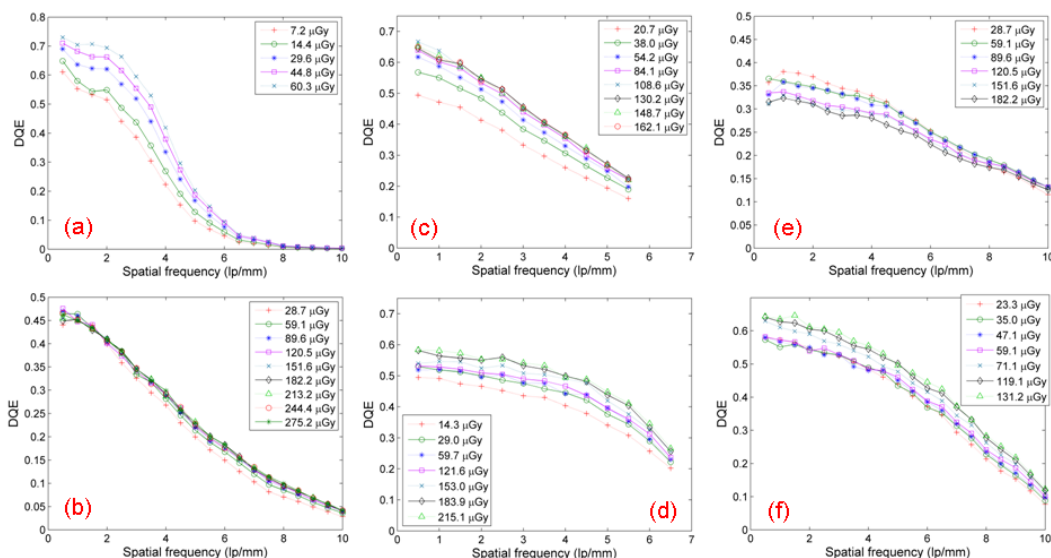
Figure 6. Average DQE curves (at 28 kV W/Al) of a) LAS, b) Hamamatsu C9732DK, c) Anrad SMAM, d) Dexela 2923MAM (HFW mode), e) Remote RadEye HR, and f) DynAMITe.

Figure 7 shows the CNR curves for the simulated breast phantoms. It was found that for Breast 1 (which is thin (5 cm) but dense (73 % granularity) -see Table 1), LAS has the highest CNR values (due to its high DQE(0.5)) for low DAK level (46.7 µGy), while Dexela has the highest one for higher DAK level (128.5 µGy). For the second breast (which is thick (6 cm) but less dense (47 % granularity - see Table 1),

LAS has again the highest CNR value, while Dexela and DynAMITe SP have the highest ones at higher DAK level. Hence, these three detectors (all based on CMOS APS technology) have the highest CNR performance.
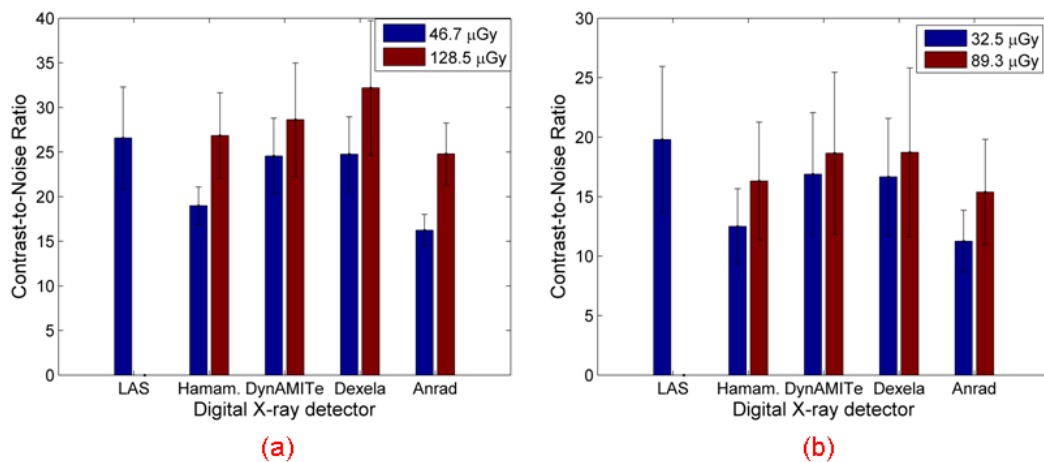
Figure 7. CNR curves for a) Breast 1 (at 46.7 and 128.5 µGy) and b) Breast 2 (at 32.5 and 89.3 µGy)

However, CNR does not take into account the spatial resolution of the detector . It depends mainly on the SNR transfer of large scale objects. Hence, contrast-detail analysis (using the CDMAM phantom) was used to evaluate the performance of the detector for different spatial frequencies. Contrast-detail analysis takes into account spatial resolution, contrast and noise (i.e. there is a relationship between contrast-detail analysis and pMTF, NNPS and DQE). At low DAK level (figure 8a), the Dexela detector has the highest performance for small disc diameter due to its high DQE values at high spatial frequencies, LAS has the highest one for medium diameters, while DynAMITe SP is the best one for large diameters (low spatial frequency). At higher DAK levels (Figure 8b), Dexela and DynAMITe SP have the best detectability for small disc diameters, while DynAMITe SP and Anrad have the highest one for large diameters. The Hamamatsu detector has low performance for both DAK levels (due to its moderated DQE values).
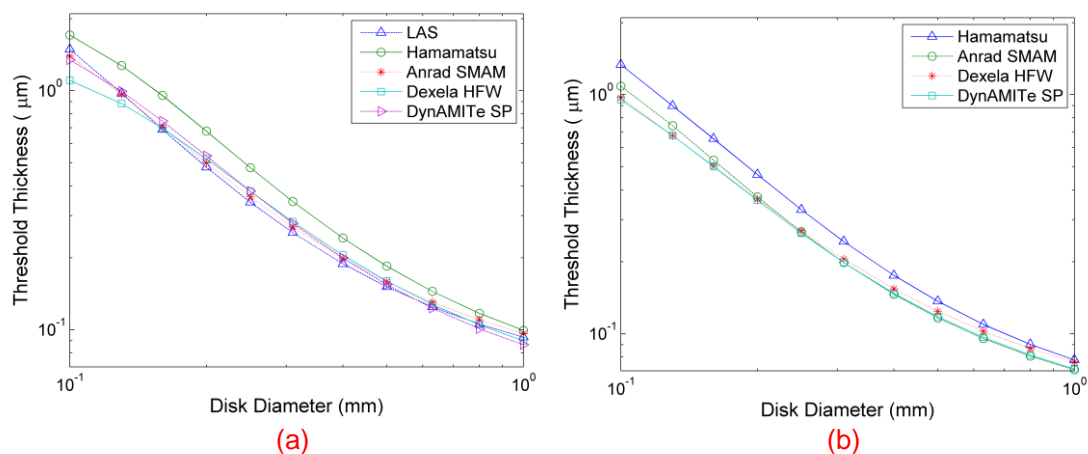
Figure 8. Threshold thickness as a function of disc diameter at a) 59 and b) 120 µGy.

Conclusion

It was found that Dexela detector (operated in HFW mode) has the best mammographic performance, because it has the best detectability of small disc diameters for low DAK levels (due to its high DQE values at high spatial frequencies). LAS and DynAMITe demonstrate high performance for medium and large disc diameters. Anrad has high detectability for large objects but limited for lower ones due to aliasing. Finally, Hamamatsu has low performance due to its moderate DQE values. It was found that LAS has the highest CNR values, but this analysis does not take into account the spatial resolution (it depends mainly on the SNR transfer of large scale objects).

Acknowledgements

References

1. Bourne R., *Fundamentals of digital imaging in medicine*, Springer-Verlag, London, 2010

2. Lança L. and Silva A. "Digital radiography detectors − A technical overview: Part 2", *Radiography*, 15, 134-138, 2009

3. Dainty, J.C. and Shaw R., *Image science: principles, analysis and evaluation of photographic-type imaging processes*, Academic Press Inc., London, 1974

4. Saunders R.S. and Samei E. "A method for modifying the image quality parameters of digital radiographic images", *Medical Physics*, 30, 3006-3017, 2003

5. Konstantinidis, A.C., *Evaluation of digital X-ray detectors for medical imaging applications*, Ph.D. thesis, University College London, London, 2011

6. *Konstantinidis A.C., Zheng Y., Olivo A., Bliznakova K., Yip M., Anaxagoras T., Wells K., Allinson N., and Speller R.D.: "Evaluation of a Novel Wafer-Scale CMOS APS X-Ray Detector for Use in Mammography", IEEE Nuclear Science Symposium and Medical Imaging Conference (NSS-MIC), Anaheim, California, USA, October 29 - November 3,* pp. 3254-3260, 2012

7. Konstantinidis A.C., Olivo A. and Speller RD. "Technical Note: Further development of a resolution modification routine for the simulation of the modulation transfer function (MTF) of digital X-ray detectors", *Medical Physics*, 38, 5916-5920, 2011

8. Bliznakova K., Suryanarayanan S., Karellas A., and Pallikarakis N. "Evaluation of an improved algorithm for producing realistic 3D breast software phantoms: Application for mammography", *Medical Physics*, 37, 5604-5617, 2010

9. Bliznakova K., Sechopoulos I., Buliev I., and Pallikarakis N. "BreastSimulator: A software platform for breast X-ray imaging research", *Journal of Biomedical Graphics and Computer*, 2, 1-14, 2012

10. Yip M., Alsager A., Lewis E., Wells K. and Young, K.C.: *"Validation of a digital mammography image simulation chain with automated scoring of CDMAM images", 9th International Workshop on Digital Mammography (IWDM), Tucson, USA, July 20-23*, pp. 409–416, 2008

11. Young K.C., Cook J.J.H., Oduko J.M. and Bosmans H.: *"Comparison of software and human observers in reading images of the CDMAM test object to assess digital mammography systems", SPIE Medical Imaging 2006: Physics of Medical Imaging*, *San Diego, California, USA, February 11-16*, 6142, pp. 614206, 2006

12. Rowlands J.A. "The physics of computed radiography", *Physics in Medicine and Biology*, 47, R123-R166, 2002

13. Yaffe M.J. and Rowlands J.A., "X-ray detectors for digital radiography", *Physics in Medicine and Biology*, 42, pp. 1-39, 1997

14. El Gamal A. and Eltoukhy H. "CMOS image sensors", *IEEE Circuits and Devices*, 21, pp. 6-20, 2005

15. Esposito M., Anaxagoras T., Fant A., Wells K., Konstantinidis A., Osmond J., Evans P., Speller R., and Allinson N. "DynAMITe: a wafer scale sensor for biomedical applications", *Journal of Instrumentation*, 6, pp. C12064-1–C12064-12, 2011

16. Konstantinidis A.C., Szafraniec M.B., Speller R.D., and Olivo A. "The Dexela 2923 CMOS X-ray detector: A flat panel detector based on CMOS active pixel sensors for medical imaging applications", *Nuclear Instruments and Methods in Physics Research A*, 689, pp. 12-21, 2012

17. IEC 62220-1-2, *Medical electrical equipment-characteristics of digital X-ray imaging devices: Part 1–2. Determination of the detective quantum efficiency-detectors used in mammography*, International Electrotechnical Commission (IEC), Geneva, 2007

18. Bijkerk K., Thijssen M., and Arnoldussen T., *Manual CDMAM-phantom type 3.4*, University Medical Centre, Nijmegen, 2000

19. Visser R. and Karssemeijer N., *Manual CDCOM version 1.5.2: software for automated readout of CDMAM 3.4 images*, Radboud University Nijmegen Medical Centre, Nijmegen, 2008

20. Karssemeijer N. and Thijssen M.A.O.: *"Determination of contrast-detail curves of mammography systems by automated image analysis", 3rd International Workshop on Digital Mammography (IWDM), Chicago, Illinois, USA, June 9-12*, 1119, pp. 155-160, 1996

21. Konstantinidis A.C.: *"CDMAM_FIT_3: A Graphical User Interface for Mammographic Contrast-Detail Analysis", Conference on Bio-Medical Instrumentation and related Engineering And Physical Sciences (BIOMEP 2013), June 21-22, 2013*